

Supporting Information

$^{19}\text{F}/^{119}\text{Sn}/^{207}\text{Pb}$ NMR Studies on Ion Dynamics in Tetragonal PbSnF_4 ; Spectroscopic Evidence for Defect-Driven Conductivity

Miwa Murakami,^{1,*} Yoshiyuki Morita¹, and Motohiro Mizuno²

¹Office of Society-Academia Collaboration for Innovation, Kyoto University, Uji,
Kyoto, 611-0011, Japan.

²Department of Chemistry, Graduate School of Natural Science and Technology,
Kanazawa University, Kanazawa 920-1192, Japan.

* email m-murakami@saci.kyoto-u.ac.jp

Gokasho, Uji, Kyoto 611-0011, Japan

Tel: +81-774-38-4967, Fax: +81-774-38-4996

Contents

Table S1. Crystal and Refinement Parameters for $\beta\text{-PbSnF}_4$

Table S2. Structural Parameters for $\beta\text{-PbSnF}_4$

Table S3. Anisotropic Thermal Parameters

Figure S1. Fitted neutron diffraction profile for $\beta\text{-PbSnF}_4$.

Figure S2. Thermal ellipsoid plots (30 % probability) of $\beta\text{-PbSnF}_4$ in the unit cell.

Figure S3. Contribution of the dipolar relaxation and the CSA relaxation to the temperature dependence of the ^{207}Pb spin-lattice relaxation time for $\beta\text{-PbSnF}_4$.

Figure S4. Experimental and calculated ^{119}Sn MAS spectra. Some details about simulation algorithm are also given.

Table S1. Crystal and Refinement Parameters for β -PbSnF₄

Crystal system	Tetragonal
Space group	<i>P4/nmm</i>
Unit cell dimensions	$a = 4.23629(10) \text{ \AA}$ $c = 11.45875(55) \text{ \AA}$
Volume	205.6408(121)
<i>Z</i>	2
Calculated density	6.490736 g/cm ³
<i>R</i> factors	$R_p = 0.06366$ $R_{wp} = 0.09572$ $R_{ex} = 0.02835$ $R_F^2 = 0.08988$
# of profile points used	1791

Table S2. Structural Parameters for β -PbSnF₄

atom	<i>x</i>	<i>y</i>	<i>z</i>	U_{iso}
Pb	0.750000	0.750000	0.37861(58)	0.020279
Sn	0.250000	0.250000	0.13375(75)	0.011331
F1	0.750000	0.250000	0.20838(135)	0.247351
F2	0.750000	0.250000	0.50000	0.021116
F3	0.250000	0.250000	0.31554(105)	0.189801

Table S3. Anisotropic Thermal Parameters

atom	U_{11}	U_{22}	U_{33}	U_{12}	U_{13}	U_{23}
Pb	0.01870	0.01870	0.02343	0.00000	0.00000	0.00000
Sn	0.01676	0.01676	0.00047	0.00000	0.00000	0.00000
F1	0.02306	0.35947	0.35952	0.00000	0.00000	0.00000
F2	0.01152	0.01152	0.04032	0.00000	0.00000	0.00000
F3	0.25740	0.25740	0.05460	0.00000	0.00000	0.00000

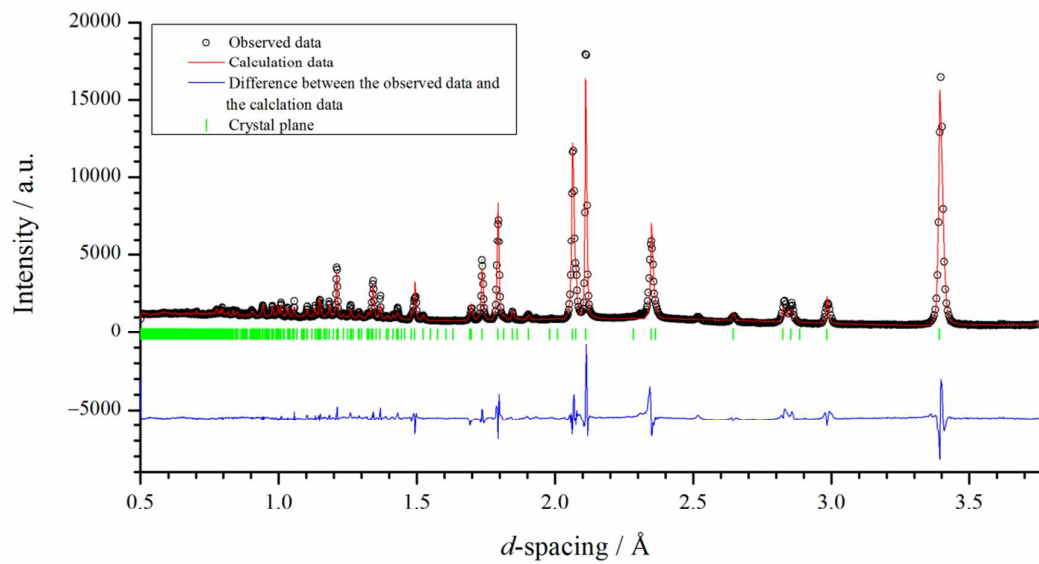


Figure S1. Fitted neutron diffraction profile for β -PbSnF₄.

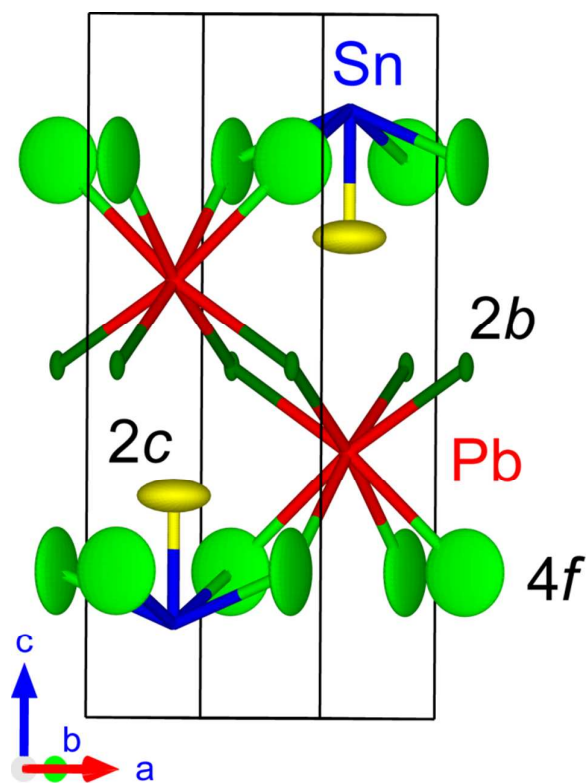


Figure S2. Thermal ellipsoid plots (30 % probability) of β -PbSnF₄ in the unit cell. *a*, *b*, and *c* denotes three crystallographic axes. Blue and red balls are Pb and Sn, respectively. The three F sites (2b, 2c, and 4f) are designated by dark green, yellow, and green ellipsoids, respectively.

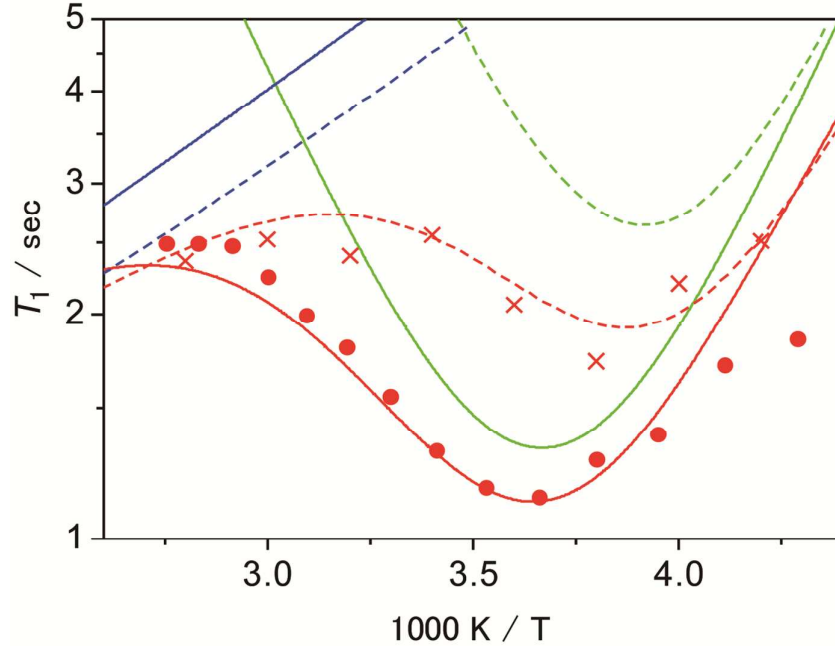


Figure S3. Contribution of the dipolar relaxation and the CSA relaxation to the temperature dependence of the ^{207}Pb spin-lattice relaxation time (T_1) for $\beta\text{-PbSnF}_4$. The filled circles denote the observed T_1 at 14 T and the cross at 7 T. The red solid and dotted curves through the data points are the calculated sum of the two relaxation rate, $(\frac{1}{T_1})_{\text{D}} + (\frac{1}{T_1})_{\text{CSA}}$, the blue curves are $(\frac{1}{T_1})_{\text{D}}$, and the red ones are $(\frac{1}{T_1})_{\text{CSA}}$. The solid lines are for 14 T and the dotted ones are for 7 T. Each rate function is given in the text, and the parameters for calculation were $A_{\text{D}} = 2.0 \times 10^8 / \text{s}^{-2}$, τ_0 and E_{a} for the dipolar fluctuation = $8 \times 10^{-10} / \text{s}$ and 7.7 kJ/mol, respectively, and τ_0 and E_{a} for the CSA relaxation = $5 \times 10^{-14} / \text{s}$ and 23 kJ/mol, respectively. A_{CSA} corresponds to $\Delta\sigma(1+\eta^2/3)^{-1/2} = 120 \text{ ppm}$ with Eq. (6) in the text.

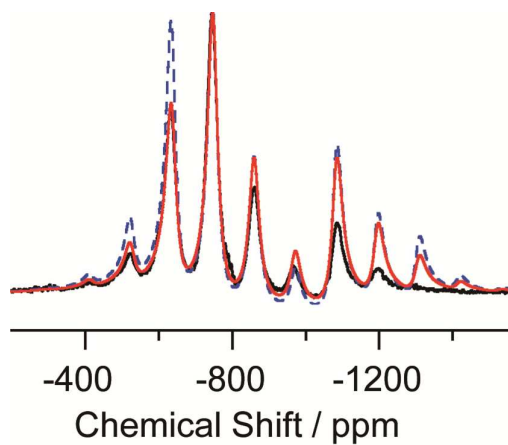


Figure S4. Observed (black) and calculated (red and blue-dotted) ^{119}Sn MAS spectra of $\beta\text{-PbSnF}_4$ taken at 25 °C with the MAS frequency of 25 kHz. The CSA parameters obtained from the static spectrum at -40 °C ($\sigma_{11} = -534$ ppm, $\sigma_{22} = -633$ ppm, and $\sigma_{33} = -1412$ ppm) were used to calculate the spectrum given in the blue-dotted line. The spectrum given in the red line was calculated with these CSA parameters and the 4-site motion of the σ_{33} axis schematically illustrated in Fig. 2(b) with the apex angle of 34° and the rate $> 10^7$ Hz. Apodization by an exponential broadening function (7 kHz) was applied to the calculated FID data before Fourier transformation.

It is notable that the calculated static lineshape (the blue-dotted line) is not consistent with the observed one, while the agreement is better for the calculated one with including motion (the red line). Due most probably to the neglect of the Hahn-echo process in calculation, the observed intensities of the spinning sidebands at the lower-frequency sides are smaller than those calculated one appreciably. As it is difficult to incorporate the Hahn-echo process, molecular motion, and MAS into the simulation program, we have not tried to fit the MAS spectra

Some details about simulation algorism

Simulated ^{119}Sn NMR spectra were produced with FORTRAN original programs [1,2]. For the wobbling motion, 4-site jump was assumed. NMR frequency at site i was calculated as [3,4]

$$\omega_{CSi} = \sqrt{\frac{2}{3}} \sum_{n,m=-2}^2 D_{n0}^{(2)}(\psi, \theta, \phi) D_{mn}^{(2)}(\alpha_i, \beta_i, \gamma_i) \rho_{2m}^{CS}, \quad (1)$$

$$\rho_{20}^{CS} = \sqrt{\frac{3}{2}} \left(\sigma_{33} - \frac{1}{3} \text{Tr} \hat{\sigma} \right), \quad \rho_{2\pm 2}^{CS} = \frac{1}{2} (\sigma_{11} - \sigma_{22}), \quad (2)$$

where $D_{mn}^{(2)}(\Omega)$ is the second-order Wigner rotation matrix. $(\alpha_i, \beta_i, \gamma_i)$ and (ψ, θ, ϕ) are the Euler angles for transformation from the principal axes of the chemical shift tensor to the molecular axes and from the molecular axes to the laboratory axes, respectively.

The echo signal $G(t, \theta, \phi)$ is written as

$$G(t, \theta, \phi) = \mathbf{1} \cdot \hat{\mathbf{B}} \exp(\hat{\mathbf{A}} t) \exp(\hat{\mathbf{A}} \tau) \exp(\hat{\mathbf{A}}^* \tau) \cdot \mathbf{P}, \quad (3)$$

where $\hat{\mathbf{A}}$ is the matrix with the elements $i\omega_i - k_{ii}$ on the diagonal and k_{ij} off the diagonal. k_{ij} is the jumping rate between site i and j . $\hat{\mathbf{B}}$ and \mathbf{P} are the matrix for finite pulse width and a vector of site populations, respectively. $\mathbf{1}$ is a vector written as $\mathbf{1} = (1, 1, 1, 1)$.

The signal of a powder sample was calculated by

$$G(t) = \int_0^{2\pi} \int_0^{2\pi} G(t, \theta, \phi) \sin \theta d\theta d\phi. \quad (4)$$

The simulation spectrum was obtained by Fourier transform of $G(t)$.

NMR frequency at site i for a sample under MAS is written as

$$\omega_{CSi} = \sqrt{\frac{2}{3}} \sum_{n,k,m=-2}^2 D_{n0}^{(2)}(0, \theta_m, \omega_r t) D_{kn}^{(2)}(\alpha, \beta, \gamma) D_{mk}^{(2)}(\alpha_i, \beta_i, \gamma_i) \rho_{2m}^{CS}, \quad (5)$$

where $\theta_m (= \cos^{-1} 1/\sqrt{3})$ is the magic angle and ω_r is the sample spinning speed. $(\alpha_i, \beta_i, \gamma_i)$ and (α, β, γ) are the Euler angles for transformation from the principal axes of the chemical shift tensor to the molecular axes and from the molecular axes to the rotor axes, respectively.

The time evolution of the magnetization $M(t)$ is represented by [5]

$$M(t) = \hat{\mathbf{L}}(t) \cdot \mathbf{P}, \quad (6)$$

$$\hat{\mathbf{L}}(t) = T \exp \left[\int_0^t \hat{\mathbf{A}}(t') dt' \right], \quad (7)$$

where T is the Dyson time-ordering operator.

Here, equal time increment Δt such that $t = n\Delta t$ is considered. By assuming time-independent $\hat{\mathbf{A}}(t)$ for a short period of time Δt , $\hat{\mathbf{L}}(t)$ is written as

$$\hat{\mathbf{L}}(t) = \hat{\mathbf{L}}(n\Delta t) = T \prod_{n'=1}^n \hat{\mathbf{S}}((n'-1)\Delta t) \exp \left[\hat{\mathbf{A}}((n'-1)\Delta t) \Delta t \right] \hat{\mathbf{S}}((n'-1)\Delta t)^{-1}, \quad (8)$$

$$\hat{\mathbf{A}}((n'-1)\Delta t) = \hat{\mathbf{S}}((n'-1)\Delta t)^{-1} \hat{\mathbf{A}}((n'-1)\Delta t) \hat{\mathbf{S}}((n'-1)\Delta t), \quad (9)$$

where $\hat{\mathbf{S}}((n'-1)\Delta t)$ is the matrix which transforms $\hat{\mathbf{A}}((n'-1)\Delta t)$ into a diagonal matrix

$\hat{\mathbf{A}}((n'-1)\Delta t)$. When one rotor period is divided into n_{rot} equal periods Δt , the following relation is obtained

$$\exp \left[\hat{\mathbf{A}}((n_{\text{rot}} + 1)\Delta t) \Delta t \right] = \exp \left[\hat{\mathbf{A}}(\Delta t) \Delta t \right]. \quad (10)$$

Once $\hat{\mathbf{A}}((n'-1)\Delta t)$ and $\hat{\mathbf{S}}((n'-1)\Delta t)$ are estimated over one rotor period, $\hat{\mathbf{L}}(t)$ at subsequent times are calculated using these matrices and eq.(10). The NMR signal is given by

$$G(\alpha, \beta, \gamma, t) = \mathbf{1} \cdot \hat{\mathbf{B}} \cdot \hat{\mathbf{L}}(t) \cdot \mathbf{P} \quad (11)$$

The signal of a powder sample was calculated by

$$G(t) = \int_0^{2\pi} \int_0^\pi \int_0^{2\pi} G(\alpha, \beta, \gamma, t) \sin \beta d\alpha d\beta d\gamma. \quad (12)$$

The simulation spectrum was obtained by Fourier transform of $G(t)$. Note here that we did not take the Hahn-echo process in the MAS simulation and hence the fitting in Figure S4 was not satisfactorily.

- [1] Araya, T.; Niwa, A.; Mizuno, M.; Endo, K. Dynamics of $[\text{Sn}(\text{D}_2\text{O})_6]^{2+}$ in $[\text{Zn}(\text{D}_2\text{O})_6][\text{SiF}_6]$ Crystal as Studied by 1D, 2D Spectra and Spin-lattice Relaxation Time of ^2H NMR. *Chem. Phys.* **2008**, *344*, 291-298.
- [2] Mizuno, M.; Suzuki, Y.; Endo, K.; Murakami, M.; Tansho, M.; Shimizu, T. Molecular Dynamics in Paramagnetic Materials as Studied by Magic-Angle Spinning ^2H NMR Spectra. *J. Phys. Chem. A* **2007**, *111*, 12954-12960.

- [3] Schmidt-Rohr, K.; Spiess, H. W. *Multidimensional Solid-State NMR and Polymers*; Academic Press: London, 1994.
- [4] Vold, R. R. In *Nuclear Magnetic Resonance Probes of Molecular Dynamics*; Tycko, R., Ed.; Kluwer Academic Publishers: Norwell, MA, 1994; pp 27-112.
- [5] Duer, M. J.; Levitt, M. H. Time-Domain Calculation of Chemical Exchange Effects in the NMR Spectra of Rotating Solids. *Solid State Nucl. Magn. Reson.* **1992**, *1*, 211-215.